nature

LETTERS

Direct observation of second-order atom tunnelling

S. Fölling[1], S. Trotzky[1], P. Cheinet[1], M. Feld[1], R. Saers[2], A. Widera[1,3], T. Müller[1,4] & I. Bloch[1]

Tunnelling of material particles through a classically impenetrable barrier constitutes one of the hallmark effects of quantum physics. When interactions between the particles compete with their mobility through a tunnel junction, intriguing dynamical behaviour can arise because the particles do not tunnel independently. In single-electron or Bloch transistors, for example, the tunnelling of an electron or Cooper pair can be enabled or suppressed by the presence of a second charge carrier due to Coulomb blockade[1,2]. Here we report direct, time-resolved observations of the correlated tunnelling of two interacting ultracold atoms through a barrier in a double-well potential. For the regime in which the interactions between the atoms are weak and tunnel coupling dominates, individual atoms can tunnel independently, similar to the case of a normal Josephson junction. However, when strong repulsive interactions are present, two atoms located on one side of the barrier cannot separate[3], but are observed to tunnel together as a pair in a second-order co-tunnelling process. By recording both the atom position and phase coherence over time, we fully characterize the tunnelling process for a single atom as well as the correlated dynamics of a pair of atoms for weak and strong interactions. In addition, we identify a conditional tunnelling regime in which a single atom can only tunnel in the presence of a second particle, acting as a single atom switch. Such second-order tunnelling events, which are the dominating dynamical effect in the strongly interacting regime, have not been previously observed with ultracold atoms. Similar second-order processes form the basis of superexchange interactions between atoms on neighbouring lattice sites of a periodic potential, a central component of proposals for realizing quantum magnetism[4–7].

For the description and observation of quantum mechanical tunnelling, a double-well-type potential, where two localized spatial modes are separated by a barrier, is among the conceptually simplest set-ups. When a particle is initially prepared on one side of this barrier, it will tunnel back and forth between the two sides with a well-defined frequency. For macroscopic quantum systems, such as superconductors or atomic Bose–Einstein condensates, this tunnel coupling can lead to a Josephson-type tunnelling dynamics[8–10]. When interactions between individual particles are much stronger than the tunnel coupling in the system, quantized Josephson dynamics arises—in which, for example, the charge carriers in superconducting devices tunnel individually across barriers[11,12].

In the case of coupled mesoscopic quantum dots, a co-tunnelling regime can be achieved, where separate electrons only tunnel in a correlated way[13,14]. For ensembles of ultracold atoms in periodic potentials, strong interactions fundamentally alter the properties of the many-body system, leading to strongly correlated phases such as the Mott insulating state[15–19]. In such cases, where direct first-order tunnelling of single atoms is highly suppressed, second-order correlated tunnelling processes can be the dominant dynamical effects. Despite the absence of direct long-range interaction mechanisms between particles, second-order "superexchange"-type processes

can provide effective spin-dependent interactions between particles at separate positions[4–7].

The dynamics of interacting bosonic atoms in a double well with tight confinement is described by a quantized Josephson or a two-mode Bose–Hubbard hamiltonian[11,12]

$$H = -J\left(\hat{a}_L^\dagger \hat{a}_R + \hat{a}_R^\dagger \hat{a}_L\right) - \frac{1}{2}\Delta(\hat{n}_L - \hat{n}_R) + \frac{1}{2}U(\hat{n}_L(\hat{n}_L - 1) + \hat{n}_R(\hat{n}_R - 1)) \quad (1)$$
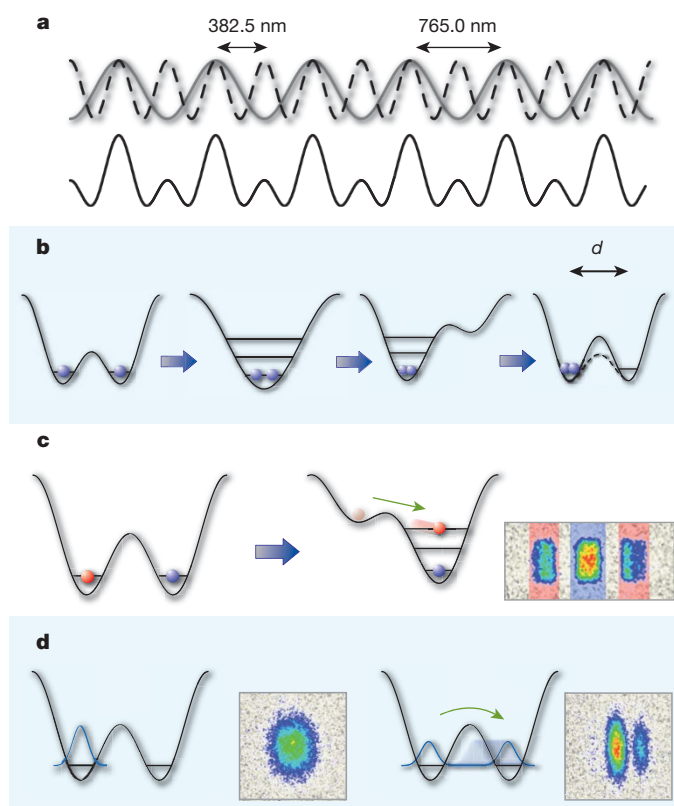

Figure 1 | Schematics of double-well generation, loading and detection sequences. a, Superimposing two optical lattice potentials differing in period by a factor of two creates an array of double-well potentials. **b,** Preparation sequence. An initially large well is split into a biased double-well potential such that each left well is populated. The bias is then removed and the central barrier lowered to initiate the tunnelling dynamics (d denotes the well separation). **c,** Position measurement. The atom number on each side can be recorded by 'dumping' the population of the left well into an excited vibrational state of the right well[21]. Subsequent band-mapping projects both states into separate Brillouin zones in free space[30] (marked red and blue in the inset). **d,** Interferometric detection. After sudden release from the double-well potential and a period of free expansion, the double-slit interference pattern is recorded. Particles localized to one well exhibit no interference; for delocalized atoms the pattern yields the relative single-particle phase ($-\pi/2$ in the case shown).

[1]Institut für Physik, Johannes Gutenberg-Universität, 55099 Mainz, Germany. [2]Department of Physics, Umeå University, 90187 Umeå, Sweden. [3]Institut für Angewandte Physik, Universität Bonn, 53115 Bonn, Germany. [4]Institute of Quantum Electronics, ETH Zürich, 8093 Zürich, Switzerland.

with J the tunnelling matrix element, $\hat{a}^{\dagger}_{L,R}$ and $\hat{a}_{L,R}$ the creation and annihilation operators for a bosonic particle in the ground state of the left or right well, Δ the bias potential between the wells and U the interaction energy for two particles in a single well. In the following, we assume repulsive interactions ($U > 0$); however, attractive interactions lead to a similar evolution. The operators $\hat{n}_L$ and $\hat{n}_R$ count the number of atoms in the left and right modes, respectively. In the tight-confinement approximation, the quantum state of the atoms can be described in a Fock state basis $|n_L, n_R\rangle$ with n_L and n_R being non-negative integers. For a single atom, the two possible states $|1,0\rangle$ and $|0,1\rangle$ are coupled by the tunnel matrix element J. For the case of two atoms, the states $|2,0\rangle$ and $|0,2\rangle$ both directly couple to the state $|1,1\rangle$ via the tunnelling term in first order. For strong interactions $U \gg J$, the energy difference between the states $|2,0\rangle$ and $|1,1\rangle$ is much larger than the coupling, resulting in a strong detuning and therefore in suppressed transitions between these states. For an unbiased junction ($\Delta = 0$), the state $|0,2\rangle$, however, always has the same energy as $|2,0\rangle$. The direct transition to this state, which corresponds to the co-tunnelling of both atoms as a pair, is therefore still resonant. This second-order tunnelling process has an effective matrix element $2J^2/U$, which can be obtained by second-order perturbation theory for $J/U \ll 1$ (see refs 5 and 6).

To realize the double-well potentials for ultracold rubidium atoms, we superimpose two periodic potentials with a periodicity of 382.5 nm (short lattice) and 765.0 nm (long lattice) and controllable intensities and relative phase (see Methods). They are produced by two independent optical standing waves in such a way that each potential minimum of the long lattice is split into two wells by a maximum of the short-lattice potential (see Fig. 1a). By changing the relative phase of the two potentials, a controlled bias Δ can be introduced, which can be approximated by the energy difference between the two potential minima. Additional standing waves on the two orthogonal axes provide transverse confinement, creating a three-dimensional array of up to 10^5 double wells[20] occupied by one to two ^{87}Rb atoms each. In this array we carry out many identical

instances of the experiment in parallel to obtain the quantum mechanical expectation values of the observables in a single run.

The initial state with the atoms localized on one side of the double wells is obtained by adiabatic changes of the potential after loading in the symmetric configuration. Both sites are combined and the atoms are brought to rest on the left side of their respective double well (see Fig. 1b). The tunnelling dynamics can subsequently be initiated by quickly reducing the barrier height within 200 μs. After an evolution period, we determine the resulting average position and the average single-particle phase relation between the quantum states in the left and right well. The overall sums of atoms N_L and N_R in the left and the right wells, respectively, are obtained by rapidly suppressing tunnelling again in 200 μs and employing a band mapping technique[21] (see Fig. 1c). We calibrate this method by making reference measurements with fully localized atoms prepared on either side. From the two occupation numbers the average position $\langle x \rangle = (N_R - N_L)/(N_R + N_L)$ of the particles is calculated, which denotes their position relative to the barrier in units of $d/2$, where d is the well separation. The phase relation between the two wells is determined by a separate interferometric sequence, where the lattice is switched off rapidly at the end of the dynamical evolution. The emerging double-slit matter-wave interference pattern then yields the average single-particle phase relation (see Methods and Fig. 1d).

Since approximately 40% of the population is in singly-occupied double wells, we determine the atom pair signal in a two-stage process. First the data point which includes both singly and doubly occupied wells ('total signal') is recorded for a given configuration. The measurement is then repeated with a 'filtering sequence' before the dynamical evolution period, which removes atom pairs from the trap (see Methods). By this, we obtain the single-atom signal, which can then be subtracted from the total signal to obtain the data point for atom pairs.

The time evolution for atom pairs can be calculated using the hamiltonian (1) for any given set of double-well parameters U, J and Δ within a three-state description. Our model for the ensemble
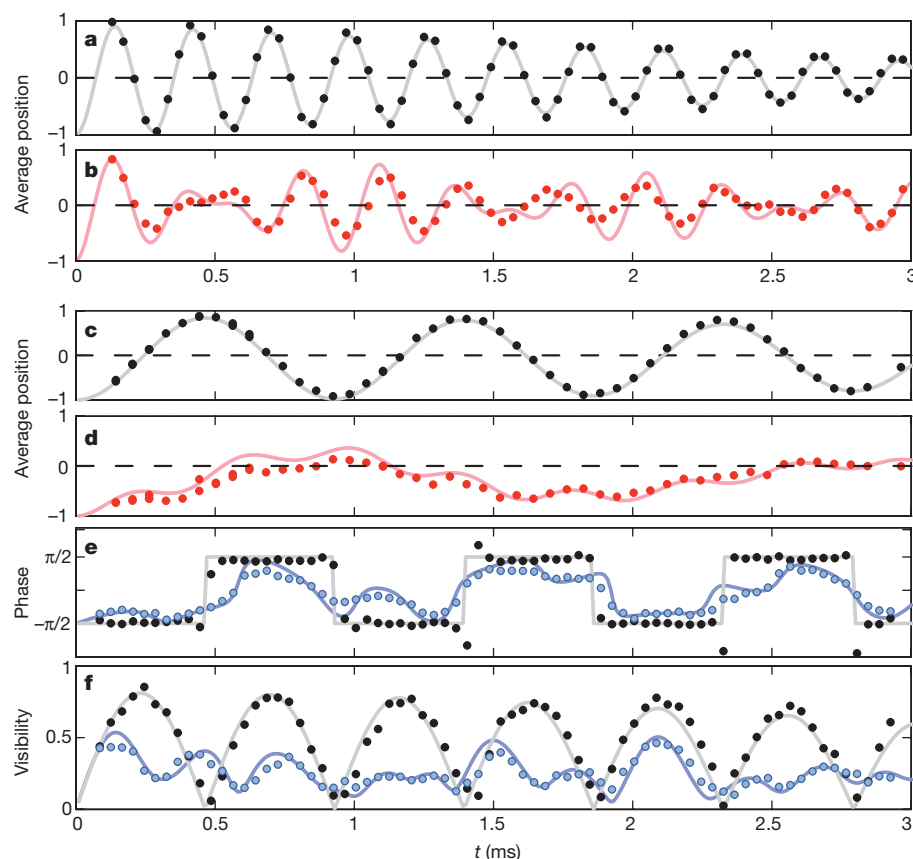

Figure 2 | Tunnelling dynamics. Full dynamical tunnelling evolution for single atoms and atom pairs in the weakly ($J/U = 1.5$) (**a**, **b**) and strongly ($J/U = 0.2$) (**c–f**) interacting regime after initially preparing all particles localized on the left side (position -1) of the double well. The black dots denote the single-atom position (**a**, **c**), phase (**e**) and visibility (**f**) signal. The red dots show the atom-pair signal (**b**, **d**). **d**, For strong interactions, first-order tunnelling is suppressed and shifted to the detuned frequency 2.5 kHz $\approx U/h$. The main dynamical process is pair tunnelling with frequency $4J^2/hU \approx 550$ Hz. **e**, **f**, Blue dots denote the combined single atom and atom pair signal recorded in the experiment by the interferometric detection method. The solid lines are fits to the data using a model based on the quantized Josephson hamiltonian (see text).
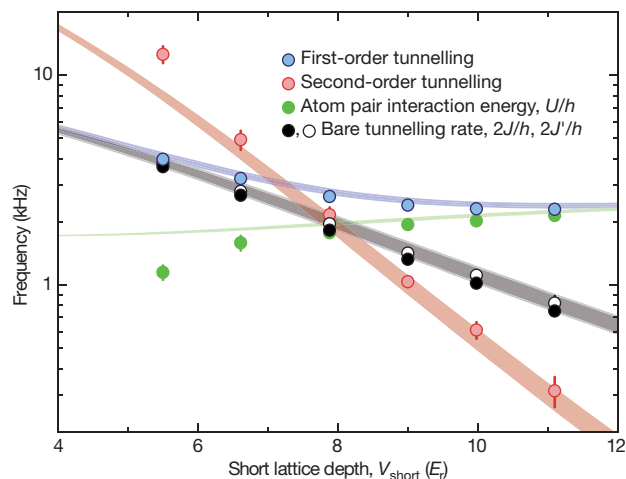
Figure 3 | Tunnelling frequencies versus short-lattice depth (barrier height). The frequencies corresponding to the coupling matrix elements J and J' (see text) are denoted with filled and unfilled black circles, respectively. The crossover above which the measured interaction energy U (green circles) dominates over kinetic energy takes place around $8E_r$. The characteristic frequencies for the second-order tunnelling process and the first-order tunnelling for atom pairs derived from these values are shown as red and blue circles, respectively. Error bars denote the 90% confidence intervals as determined from the fits. The shaded areas show the calculated frequencies for the single-atom tunnelling as well as for the first- and second-order tunnel process as determined from band structure calculations. Their width represents the systematic 2% uncertainty of the lattice depths.

takes into account inhomogeneities in the parameter Δ as well as in the atom density, owing to the overall confining potential (see Methods). We observe experimentally that the parameters in the Bose–Hubbard description in the case of pair occupation are slightly, but notably modified. Specifically, the effective tunnel coupling has to be described by a modified effective single-particle tunnelling rate J' for the two-atom hamiltonian, which is 3–10% higher than the free-particle J. This is in agreement with estimates using perturbative modifications to the wavefunction caused by the interactions.

The measured time-resolved traces resulting from single-atom and atom-pair tunnelling are shown in Fig. 2. The single atom data sets (black dots) show the expected sinusoidal population oscillation

between the two wells at a frequency $2J/h$. If the interaction energy U is smaller than the tunnel matrix element J ($J/U \approx 1.5$; Fig. 2a and b), tunnelling of a single atom out of a pair is only slightly detuned. This process therefore competes with the resonant second-order tunnel process, leading to a signal containing more than one frequency component (see Fig. 2b). When reducing J to reach the interaction-dominated regime ($J/U \approx 0.2$, Fig. 2c–f), the single-atom signal is still sinusoidal at a correspondingly lower frequency. However, the average position of atom pairs now shows a strongly modified behaviour. The pair-breaking first-order process is highly suppressed owing to the detuning by the interaction energy U, and is visible as a small modulation with a period of $\sim$400 μs (Fig. 2d). In contrast, the second-order hopping process is now the dominant dynamical effect, leading to a much slower oscillation with a period of $\sim$1.8 ms. Tunnelling is resonant in the centre of the trap; however, in double wells located away from the centre along the double-well axis, the overall confining potential leads to a bias $\Delta \neq 0$. This detuning is especially significant in the case of the second-order process, where the potential bias enters twice and the effective tunnel coupling is low. Thus, for low coupling strengths, the observed oscillation amplitude of the slow second-order process averaged over the ensemble is lower than one, but remains the dominant dynamical process.

In addition to the average centre-of-mass position, the phase and visibility as obtained from the interferometric sequence are shown (Fig. 2e, f). The average direction and velocity of the flow of atoms are characterized by the phase and visibility observables and the tunnelling parameter J. For the single-atom case, we observe distinct jumps in the phase by π, whenever the particle is localized to one side of the potential well and reverses its propagation direction. When atom pairs are included, a much more complex phase evolution emerges. By fitting the modelled dynamical evolution both for atom pairs and single atoms to the data, the tunnelling matrix elements and the interaction energies can be extracted. Figure 3 shows the fitted tunnelling frequency $2J/h$ against the short-lattice depth V_{short} in units of the recoil energy $E_r = h^2/2m\lambda^2$, with m being the mass of the atoms, h Planck's constant and $\lambda = 765$ nm the short-lattice wavelength. We fit both J and J' independently and find good qualitative agreement with the theoretical prediction for J. However, we typically measure a 5% lower coupling than predicted by a band structure calculation, a deviation which is slightly larger than expected from the uncertainties of the lattice depths. The resulting pair tunnelling
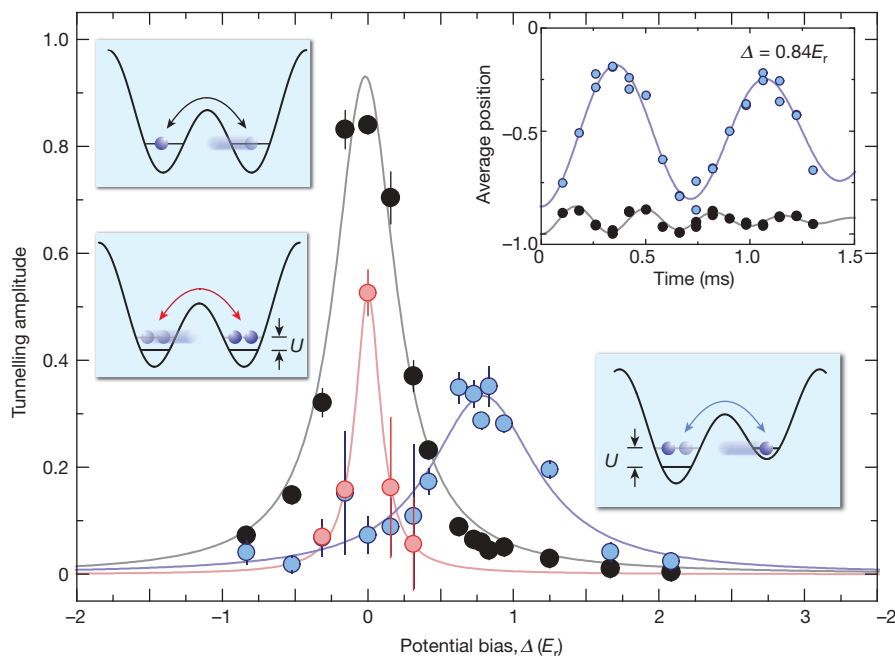

Figure 4 | Conditional tunnelling. The tunnelling amplitude versus the potential bias is measured for the case of single atoms (black data points) and initially doubly occupied lattice sites (blue and red data points) for $V_{short} = 12E_r$, with $J/U \approx 0.2$. The single-atom tunnelling (depicted in upper left inset) is only resonant in the unbiased case. For doubly occupied sites, two processes corresponding to first- and second-order tunnelling are relevant (lower right and lower left inset) and can be identified by their frequency. Each process shows a distinct resonance. The correlated pair tunnelling (red circles) is resonant for zero bias. Near a potential bias of $\Delta = 0.78(2)E_r$ (centre of lorentzian fitted to blue data points), a conditional tunnelling resonance occurs, where a single atom can tunnel only in the presence of a second atom. The dynamical evolution at this resonance can be seen in the upper right inset, where the blue (black) data points denote the average atom position versus time for the doubly (singly) occupied sites. Without a second atom the tunnelling is strongly suppressed. Amplitudes and error bars are derived from fit parameters and the uncertainties of fitting damped two-component sinusoidal functions to the position signal, as shown in the inset.

frequency $(4J'^2/U)/h$ is also plotted, showing the much faster decrease with growing barrier height compared to single-particle tunnelling. For comparison, we plot the interaction strength U as well as the expected frequency of the detuned first-order tunnelling process $\sqrt{4J'^2 + U^2}/h$, which asymptotically approaches U as $J \to 0$.

The interaction-induced suppression of first-order tunnelling for atom pairs is a consequence of energy conservation. Tunnelling can be made resonant again by biasing the single-atom ground state of the well into which the atom tunnels. If the energy offset Δ is equal to U, the first-order process is resonant in the presence of another atom, but detuned by Δ without a second atom. The signal for this conditional tunnelling process is depicted in the inset of Fig. 4, where occupation by two atoms results in a significant amplitude of the sinusoidal tunnelling signal, whereas in the case of a single atom the dynamics is barely visible. The fitted amplitudes of both processes are plotted in Fig. 4 against the bias energy, showing only one resonance at $\Delta = 0$ for single-atom occupation. The two-atom case has two resonances, one for the first-order process at $\Delta = U$ and the other at $\Delta = 0$, where the second-order hopping process is in resonance.

In conclusion, we have reported on the first full characterization of the tunnelling dynamics of an interacting atom pair across a quantum weak link. By tuning the system from a weakly to a strongly interacting regime, we have been able to observe the transition from independent single-particle tunnelling towards correlated tunnelling in second-order exchange-type processes. Our measurement shows that for higher occupations per lattice site, corrections apply to the coupling parameters of the Hubbard model as determined for a single atom. Finally, an additional correlated tunnelling regime was demonstrated, in which a particle can tunnel only on the condition of a second atom being present. Such a single atom switch can be used to efficiently create entanglement over different lattice sites. Starting from spin-triplet pairs in single wells, created for example, via spin-changing collisions[22], a resonant tunnelling event can create long-lived entangled singlet or triplet states[23]. Super-exchange interactions between neighbouring spin pairs could then be used to engineer large correlated spin-chains, similar to those encountered in cluster states[24] or resonating valence-bond-type states[25,26] of condensed matter physics.

METHODS SUMMARY

The two standing waves are produced by two independent lasers at 765 nm and 1,530 nm, respectively. Their exact wavelength ratio is set by frequency-stabilizing the beat note between the 765 nm light and a frequency-doubled fraction of the 1,530 nm beam.

Control of the relative phase of the periodic potentials at the position of the atoms is possible via the frequency offset of the lock. Dynamically shifting this phase during the state preparation sequence after the initial loading into the lattice makes it possible to prepare the initial state with all atoms on the left side of their respective double well.

The filtering sequence to obtain the pure single-atom tunnelling signal is implemented as a temporary transfer of all atoms to the $F = 2$ hyperfine manifold. During this process, two-body losses due to hyperfine-changing collisions lead to the removal of the atom pairs.

The measured data are modelled by assuming a shell-structure-type distribution of the atoms in the trap to obtain the resulting distribution of double well configurations. The evolution of the total ensemble is calculated by integrating the individual double-well signals over the distribution of bias energies Δ.

To obtain the phase and visibility data, we fit a double-slit interference pattern with gaussian envelope to the time-of-flight images obtained after sudden release of the atoms from the potential. We extract both the relative single-particle phase of the two wells and the visibility of the interference pattern. The modelled time-dependent phase and visibility signal is then fitted to this data to obtain the Hubbard model parameters U, J and Δ.

1.   Averin, D. V. & Likharev, K. K. Coulomb blockade of single-electron tunneling, and coherent oscillations in small tunnel junctions. *J. Low-Temp. Phys.* **62**, 345–373 (1986).
2.   Kouwenhoven, L. P. *et al.* in *Mesoscopic Electron Transport* (eds Sohn, L. L., Kouwenhoven, L. P. & Schön, G.) 105–214 (Kluwer, Dordrecht, 1997).
3.   Winkler, K. *et al.* Repulsively bound atom pairs in an optical lattice. *Nature* **441**, 853–856 (2006).
4.   Auerbach, A. *Interacting Electrons and Quantum Magnetism* (Springer, Berlin, 1998).
5.   Duan, L.-M., Demler, E. & Lukin, M. Controlling spin exchange interactions of ultracold atoms in an optical lattice. *Phys. Rev. Lett.* **91**, 090402 (2003).
6.   Kuklov, A. & Svistunov, B. Counterflow superfluidity of two-species ultracold atoms in a commensurate optical lattice. *Phys. Rev. Lett.* **90**, 100401 (2003).
7.   Altman, E., Hofstetter, W., Demler, E. & Lukin, M. Phase diagram of two-component bosons on an optical lattice. *New J. Phys.* **5**, 113.1–113.19 (2003).
8.   Josephson, B. D. Possible new effects in superconductive tunnelling. *Phys. Lett.* **1**, 251–253 (1962).
9.   Likharev, K. K. Superconducting weak links. *Rev. Mod. Phys.* **51**, 101–159 (1979).
10. Albiez, M. *et al.* Direct observation of tunneling and nonlinear self-trapping in a single bosonic Josephson junction. *Phys. Rev. Lett.* **95**, 010402 (2005).
11. Averin, D. V. Quantum computing and quantum measurement with mesoscopic Josephson junctions. *Fortschr. Phys.* **48**, 1055–1074 (2000).
12. Makhlin, Y., Schön, G. & Shnirman, A. Quantum-state engineering with Josephson-junction devices. *Rev. Mod. Phys.* **73**, 357–400 (2001).
13. De Franceschi, S. *et al.* Electron cotunneling in a semiconductor quantum dot. *Phys. Rev. Lett.* **86**, 878–881 (2001).
14. Zumbühl, D. M., Marcus, C. M., Hanson, M. P. & Gossard, A. C. Cotunneling spectroscopy in few-electron quantum dots. *Phys. Rev. Lett.* **93**, 256801–256804 (2004).
15. Fisher, M. P. A., Weichman, P. B., Grinstein, G. & Fisher, D. S. Boson localization and the superfluid-insulator transition. *Phys. Rev. B* **40**, 546–570 (1989).
16. Jaksch, D., Bruder, C., Cirac, J. I., Gardiner, C. W. & Zoller, P. Cold bosonic atoms in optical lattices. *Phys. Rev. Lett.* **81**, 3108–3111 (1998).
17. Greiner, M., Mandel, O., Esslinger, T., Hänsch, T. W. & Bloch, I. Quantum phase transition from a superfluid to a Mott insulator in a gas of ultracold atoms. *Nature* **415**, 39–44 (2002).
18. Spielman, I. B., Phillips, W. D. & Porto, J. V. Mott-insulator transition in a two-dimensional atomic Bose gas. *Phys. Rev. Lett.* **98**, 080404 (2007).
19. Stöferle, T., Moritz, H., Schori, C., Köhl, M. & Esslinger, T. Transition from a strongly interacting 1D superfluid to a Mott insulator. *Phys. Rev. Lett.* **92**, 130403 (2004).
20. Anderlini, M., Sebby-Strabley, J., Kruse, J., Porto, J. V. & Phillips, W. D. Controlled atom dynamics in a double-well optical lattice. *J. Phys. B* **39**, S199–S210 (2006).
21. Sebby-Strabley, J. *et al.* Preparing and probing atomic number states with an atom interferometer. *Phys. Rev. Lett.* **98**, 200405 (2007).
22. Widera, A. *et al.* Coherent collisional spin dynamics in optical lattices. *Phys. Rev. Lett.* **95**, 190405 (2005).
23. Roos, C. F. *et al.* Bell states of atoms with ultralong lifetimes and their tomographic state analysis. *Phys. Rev. Lett.* **92**, 220402 (2004).
24. Briegel, H. J. & Raussendorf, R. Persistent entanglement in arrays of interacting particles. *Phys. Rev. Lett.* **86**, 910–913 (2001).
25. Anderson, P. W. The resonating valence bond state in La_2CuO_4 and superconductivity. *Science* **235**, 1196–1198 (1987).
26. Trebst, S., Schollwöck, U., Troyer, M. & Zoller, P. d-Wave resonating valence bond states of fermionic atoms in optical lattices. *Phys. Rev. Lett.* **96**, 250402–250404 (2006).
27. Myatt, C. J., Burt, E. A., Ghrist, R. W., Cornell, E. A. & Wiemann, C. E. Production of two overlapping Bose-Einstein condensates by sympathetic cooling. *Phys. Rev. Lett.* **78**, 586–589 (1997).
28. Schmaljohann, H. *et al.* Dynamics of F=2 spinor Bose-Einstein condensates. *Phys. Rev. Lett.* **92**, 040402 (2004).
29. Fölling, S., Widera, A., Müller, T., Gerbier, F. & Bloch, I. Formation of spatial shell structures in the superfluid to Mott insulator transition. *Phys. Rev. Lett.* **97**, 060403 (2006).
30. Greiner, M., Bloch, I., Mandel, O., Hänsch, T. W. & Esslinger, T. Exploring phase coherence in a 2D lattice of Bose-Einstein condensates. *Phys. Rev. Lett.* **87**, 160405 (2001).

nature

METHODS

Double-well lattice potential. The light for the two standing waves along the double-well axis is created by a 1,530 nm fibre laser and a Ti:sapphire laser running at 765 nm. The frequency relation is controlled by frequency-doubling a small part of the 1,530 nm output and recording the beat note between this light and the 765 nm lattice light. This beat note is stabilized to any offset frequency within a 1 GHz interval by a feedback circuit that adjusts the frequency of the fibre laser using a piezo-mechanical actuator. In our set-up, both laser beams are retro-reflected by a common mirror, such that the relative phase of the two periodic potentials is fixed at the mirror position. The phase slip over the distance between mirror and atoms (25 cm) caused by choosing a non-zero offset frequency allows us to control the relative phase of the two standing waves at the position of the atoms, thereby choosing the well geometry and bias energy. Typical potential depths are $9.5 E_r$ for the long lattice and $33 E_r$ for each 843 nm transversal lattice beam, in units of the 765 nm recoil energy E_r, resulting in a parabolic confinement of $\sim 2\pi \times 80$ Hz in the longitudinal direction.

State preparation. After creating an almost pure BEC of typically 8×10^4 atoms, we ramp up the optical potential within 160 ms. During the ramp, inter-double-well tunnelling is suppressed, but not the tunnelling through the barrier ($10 E_r$ final short-lattice depth). This results in a majority of the atoms being loaded into doubly-occupied sites. We then adiabatically remove the central barrier to bring the atom pairs together in one well (Fig. 1b). This well is moved to the left by half of the short-lattice period before the short lattice is ramped up again. By subsequently moving the long-wavelength lattice back to the original position we arrive again at a symmetric potential with all atoms now on the left side of their respective double well.

Filtering sequence. To obtain the tunnelling signal for single atoms, we transfer all atoms from the $F = 1$, $m_F = -1$ hyperfine state to the $F = 2$, $m_F = 0$ hyperfine state by a microwave adiabatic rapid passage after merging the wells. This strongly enhances spin relaxation collisions[22,27,28], which release enough energy to efficiently remove both atoms of each pair from the lattice. After a 40 ms hold time, the remaining atoms in singly occupied sites are transferred back to the $F = 1$, $m_F = -1$ state.

Model. To predict the time evolution of an individual double-well system, we diagonalize the hamiltonian (equation (1)) for the single-atom and the two-atom cases independently and calculate the time evolution for the two initial states $|1,0\rangle$ and $|2,0\rangle$. Owing to the gaussian shape of all lattice beams, the tunnelling, interaction and bias parameters are not perfectly identical for all double wells of the array. We assume a shell-structure distribution[29] of the atoms, with an outer region of singly occupied double wells and a spherical inner core of doubly occupied wells. This corresponds to a zero-temperature assumption. For our chosen lattice ramps and double well configuration we do not expect a perfect shell structure, but the obtained dynamical evolution is not very sensitive to changes of the distribution shape. For example, using a thermal distribution of the atoms with temperatures comparable to U/k_B and $J = 0$ gives similar results. Here, k_B denotes the Boltzmann constant. We only take into account the inhomogeneity of Δ across the cloud due to the harmonic confinement. The resulting dephasing of the ensemble is the only cause of damping of the total signal within our model. Other effects such as the inhomogeneity of the tunnelling matrix element as well as all inhomogeneities due to imperfections of the beam shapes are not included. We assume a fixed outer radius of 30 sites and use the trap frequency of the confinement and the radius of the inner shell as fitting parameters. When fitting the model to the phase and visibility data from measurements, additional sources of damping can be present. These cause an over-estimation of the trapping frequency obtained from the fit, which we observe to be up to 200%. The effect is most prominent towards the large J/U regime, where the simple three-mode approximation starts to fail. The observed damping of the position signal (Fig. 2a, b) in this regime cannot be reproduced with our model and is included by an additional, empirically determined exponential damping term with a decay time of 3.5 ms.

Phase measurement and fitting. To determine the phase relation between the wells, the trap is switched off and the interference pattern from the wavefunctions emerging from the two wells is recorded. The image is integrated perpendicularly to the double-well axis and a double-slit interference pattern with gaussian envelope is fitted to the resulting profile:

$$P(x) = A\, e^{-(x-x_0)^2/W^2}[1 + V\cos(kx + \theta)] \qquad (2)$$

The fitting parameters of the envelope are the amplitude A, the width W and average centre x_0. The interference pattern parameters are the visibility V, the periodicity k as well as the phase θ, which is directly given by the average single-particle phase relation between the wells. The momentum-space Wannier-function envelope of the measured profiles is not perfectly gaussian, especially for large tunnel coupling, leading to an overall decrease in visibility. For fitting the tunnelling dynamics model, the time-dependent signal obtained in this way is used. We simultaneously fit the signal for the total (mixed) population and for the filtered population of singly occupied double wells as shown in Fig. 2. We do not perform the atom-number-sensitive separation of the interference patterns into the signals from singly and doubly occupied sites, and model the mixed signal directly for fitting. Apart from the traces shown in Fig. 2, we typically do not record the average position for fitting, because the interference analysis yields more information per single image than the determination of the average position and the resulting data allows the determination of all parameters shown in Fig. 3.